Environ. Sci. Technol. **2005**, *39,* 1366−1377

Dendrimer Enhanced Ultrafiltration. 1. Recovery of Cu(II) from Aqueous Solutions Using PAMAM Dendrimers with Ethylene Diamine Core and Terminal NH_2 Groups

MAMADOU S. DIALLO,*,†,‡
SIMONE CHRISTIE,‡
PIRABALINI SWAMINATHAN,‡
JAMES H. JOHNSON, JR.,‡ AND
WILLIAM A. GODDARD III†

Materials and Process Simulation Center, Beckman Institute 139-74, California Institute of Technology, Pasadena, California 91125, and Department of Civil Engineering, Howard University, Washington, D.C. 20059

This article discusses the feasibility of using dendrimer enhanced ultrafiltration (DEUF) to recover Cu(II) from aqueous solutions. Building upon the results of fundamental investigations of Cu(II) binding to PAMAM dendrimers with ethylenediamine (EDA) core and terminal NH_2 groups, we combine (i) dead-end ultrafiltration (UF) experiments with (ii) atomic force microscopy (AFM) characterization of membrane fouling to assess the feasibility of using DEUF to recover Cu(II) from aqueous solutions. On a mass basis, the Cu(II) binding capacities of the EDA core PAMAM dendrimers are much larger and more sensitive to solution pH than those of linear polymers with amine groups. The dendrimer−Cu(II) complexes can be efficiently separated from aqueous solutions by ultrafiltration. The metal ion laden dendrimers can be regenerated by decreasing the solution pH to 4.0; thus enabling the recovery of the bound Cu(II) ions and recycling of the dendrimers. The UF measurements and AFM characterization studies show that EDA core PAMAM dendrimers with terminal NH_2 groups have very low tendency to foul the commercially available regenerated cellulose (RC) membranes evaluated in this study. The overall results of these experiments suggest that DEUF is a promising process for recovering metal ions such as Cu(II) from aqueous solutions.

Introduction

The discharge of toxic metal ions into surface water, groundwater, and coastal water systems has caused a major water contamination problem throughout the world (*1*). Polymer enhanced ultrafiltration (PEUF) has emerged as a promising process for recovering metal ions from contaminated water (*2*−*10*). In PEUF, a water-soluble polymer with strong binding affinity for the target metal ions is added to contaminated water. The resulting solution is passed through an ultrafiltration membrane (UF) with pore sizes smaller than those of the metal ion−polymer complexes. Highly purified permeates have been obtained using PEUF (*2*−*10*). Advances in macromolecular chemistry such as the invention of dendritic polymers are providing unprecedented opportunities to develop high-capacity nanoscale chelating agents for environmental and industrial separations. Dendritic polymers, which include random hyperbranched polymers, dendrigraft polymers, dendrons, and dendrimers, are emerging as key building blocks for a variety of nanoscale materials and technologies (*11*−*13*). They consist of globular macromolecules with three covalently bonded components: a core, interior branch cells, and terminal branch cells (*11*−*13*). Dendrimer technology has been established, which leads to either cone, spherical, or disk-like shaped "soft" nanoparticles with very low polydispersity and sizes in the range of 2−20 nm (*11*−*13*). These nanoparticles can be functionalized with surface groups that make them soluble in appropriate media or bind onto appropriate surfaces (*11*−*13*). Alternatively, they can also be covalently linked to each other to form high molecular weight megamers commonly referred to as core−shell tecto(dendrimers) (*12*).

Poly(amidoamine) (PAMAM) dendrimers were the first class of dendritic polymers to be commercialized (*11*−*13*). PAMAM dendrimers with ethylenediamine (EDA) core and terminal NH_2 groups (the initial focus of this research) are synthesized via a two-step iterative reaction sequence that produces concentric shells of β-alanine units (commonly referred to as generations) around the central EDA initiator core (Figure 1). Selected physicochemical properties of these dendrimers are given in Table 1. A number of key features make PAMAM dendrimers particularly unique as chelating agents. First, their high density of nitrogen ligands along with the possibility of attaching functional groups such as primary amines, carboxylates, hydroxymates, etc. to PAMAM dendrimers can result in a substantial increase in binding capacity for a variety of toxic metal ions [e.g., Cu(II), Ag(I), Fe(III), etc.] (*14*−*22*). The well-defined molecular compositions, sizes, and shapes of PAMAM dendrimers have also made them particularly attractive as (i) scaffolds for paramagnetic metal ions in magnetic resonance imaging (*23*−*25*) and (ii) templates for the synthesis of metal-bearing nanoparticles with electronic, optical, catalytical, and biological activity (*26*−*35*). Conventional models of complexation have typically described metal ion chelation in aqueous solutions as a set of successive reactions between a central

TABLE 1. Selected Properties of EDA Core G*x*-NH_2 PAMAM Dendrimers Evaluated in This Study

dendrimer	M_{wth} (Da)[a]	N_{NT}[b]	N_{NH2}[c]	pK_{NT}[d]	pK_{NH2}[e]	R_G (nm)[f]	R_H (nm)[g]
G3-NH_2	6906	30	32	6.52	9.90	1.65	1.75
G4-NH_2	14 215	62	64	6.85	10.29	1.97	2.5
G5-NH_2	28 826	126	128	7.16	10.77	2.43	2.72

[a] M_{wth}, theoretical molecular weight. [b] N_{NT}, number of tertiary amine groups. [c] N_{NH2}, number of primary amine groups. [d] pK_{NT}, pK_a of dendrimer tertiary amine groups (*15*). [e] pK_{NH2}, pK_a of dendrimer primary amine groups (*15*). [f] R_G, dendrimer radius of gyration. For a dendritic polymer with N atoms and molar mass M, $R_G = (1/M\langle||_{i=1}^{N} m_i|r_i - R|^2|\rangle|^{0.5})$; where R is the center-of-mass of the dendrimer, and r_i and m_i are respectively the position and mass of atom i of the dendrimer (*43*). The R_G of the EDA Core G*x*-NH_2 PAMAM dendrimers were estimated from small angle neutron scattering experiments (*45*). [g] R_H, dendrimer hydrodynamic radius. It is usually estimated using Einstein's viscosity relation $R_H = (|\eta M/10\pi N)$ (*44*); where M is the molar mass of the particle/macromolecule, η is the intrinsic viscosity of its aqueous solution, and N is Avogadro's number. The R_H of the EDA core G*x*-NH_2 PAMAM dendrimers was estimated from dilute solution viscosity measurements (*45*).

* Corresponding author phone: (626)395-2730; fax: (626)585-0918; e-mail: diallo@wag.caltech.edu.
† California Institute of Technology.
‡ Howard University.

10.1021/es048961r CCC: $30.25
Published on Web 01/22/2005

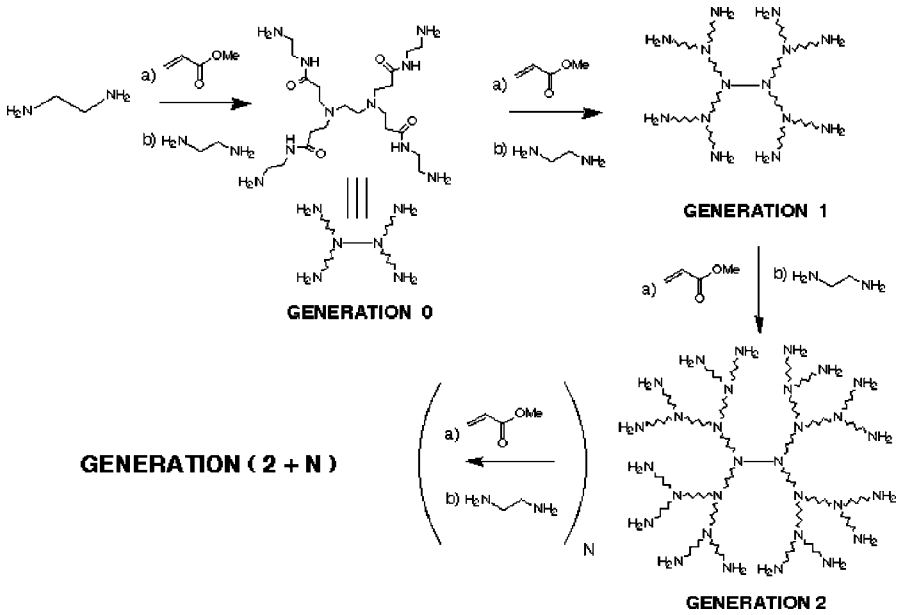

FIGURE 1. Structures of PAMAM dendrimers with EDA core and NH_2 terminal groups (*14*).

TABLE 2. Cu(II) Binding Capacity (mg/g) of G*x*-NH_2 EDA Core PAMAM Dendrimers and Linear Polymers with Amine Groups in Aqueous Solutions

	binding capacity		
chelating ligand	**pH = 9.0**	**pH = 6−8.0**	**pH = 2.0−5.0**
G3-NH_2 PAMAM[a]	420.0	333.0 (pH = 7.0)	0
G4-NH_2 PAMAM[a]	451.0	329.0 ± 8.0 (pH = 7.0)	0
G5-NH_2 PAMAM[a]	395.31	308.0 ± 20.0 (pH = 7.0)	0
poly(ethyleneimine)[b]	na[c]	153.0 (pH = 6.0)	55 (pH = 2.4)−189 (pH = 4.0)
poly(ethylene pyridine 2-aldimine)[b]	na	120.0 (pH = 6.0)	na
poly(ethylene aminodiacetic acid)[b]	na	120.0 (pH = 6.0)	na

[a] The Cu(II) binding capacity (mg/g) of the G*x*-NH_2 EDA core PAMAM dendrimers was estimated from their measured Cu(II) extents of binding (*15*). [b] The Cu(II) binding capacity of the linear polymers with amine groups were taken from Geckeler and Volchek (*2*). [c] na, not available.

metal ion (M), a ligand (L), and the proton (H^+) or hydroxide ion (OH^-) (*15*, *36*). The stability constants of a given metal ion can be determined by fitting experimental data to the corresponding chemical equilibrium and mass balance equations. Although this approach has worked well for a small ligand with a limited number of Lewis base donors (e.g., a polydendate ligand or a macrocycle), it is not feasible for nanoscale ligands with a large number of metal ion binding sites such as proteins and dendrimers (*15*, *36*).

Diallo et al. (*15*) have recently carried out an extensive study of proton binding and Cu(II) complexation in aqueous solutions of EDA core PAMAM dendrimers of different generations (G3-NH_2, G4-NH_2, and G5-NH_2) and terminal groups [G4 PAMAM dendrimers with succinamic acid ($NHCOCH_2CH_2COOH$) terminal groups, glycidyol ($NHCH_2$-$CH(OH)CH_2OH$) terminal groups, and acetamide ($NHCOCH_3$) terminal groups]. In consistence with Tanford's theory of solute binding to macromolecules (*37*), they successfully used the extent of binding (EOB) to quantify Cu(II) uptake by the PAMAM dendrimers in aqueous solutions. The EOB of metal ions in aqueous solutions of dendrimers are readily measured by (i) mixing and equilibrating aqueous solutions of metal ion + dendrimer, (ii) separating the metal ion laden dendrimers from the aqueous solutions by ultrafiltration (UF), and (iii) measuring the metal ion concentrations of the equilibrated solutions and filtrates by atomic absorption spectrophotometry (*14*, *15*). Table 2 compares the EOB of Cu(II) in aqueous solutions of EDA core G*x*-NH_2 PAMAM dendrimers to the Cu(II) binding capacities of selected linear polymers with amine groups. On a mass basis, the EOB of Cu(II) to the G*x*-NH_2 PAMAM dendrimers are much larger and more sensitive to solution pH than those of linear polymers with amine groups that have been used in previous PEUF studies (*2*). Figure 2 provides a compelling evidence of the role of tertiary amine groups in the uptake of Cu(II) by EDA core PAMAM dendrimers in aqueous solutions (*15*). Both the G4-NH_2 and G4-Ac EDA core PAMAM dendrimers have 62 tertiary amine groups with a pK_a of 6.75−6.85 (*15*). However, the G4-NH_2 PAMAM dendrimer has 64 terminal groups with a pK_a of 10.20. Conversely, the G4-Ac PAMAM dendrimer has 64 non-ionizable terminal acetamide ($NHCOCH_3$) groups. At pH 5.0, all the primary and tertiary amine groups of PAMAM dendrimers become protonated (*15*). Not surprisingly, Figure 2 shows that no binding of Cu(II) occurs at pH 5 for both the G4-NH_2 and G4-Ac PAMAM dendrimers. Conversely, significant binding of Cu(II) is observed when a significant fraction or all of the dendrimer tertiary amine groups become unprotonated at pH 7.0 and pH 9.0 (*15*).

To gain insight into metal ion coordination with the tertiary amine groups of PAMAM dendrimers, Diallo et al. (*15*) employed extended X-ray absorption fine structure (EXFAS) spectroscopy to probe the structures of aqueous complexes of Cu(II) with EDA core G*x*-NH_2 PAMAM dendrimers at pH 7.0. Analysis of the EXAFS spectra suggests the formation of octahedral complexes in which a Cu(II) central metal ion is coordinated to four dendrimer tertiary amine groups and two axial water molecules inside the dendrimers. To account for the Cu(II) ions that are not specifically bound

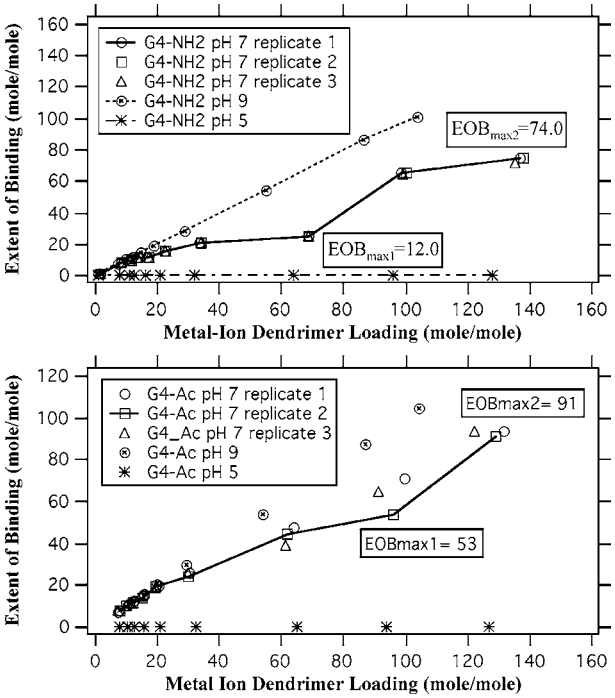

FIGURE 2. Extent of binding of Cu(II) in aqueous solutions of EDA core G4-NH_2 and G4-Ac($NHCOCH_3$) PAMAM dendrimers as a function of metal ion dendrimer loading and solution pH. Data are taken from Diallo et al. (*15*).

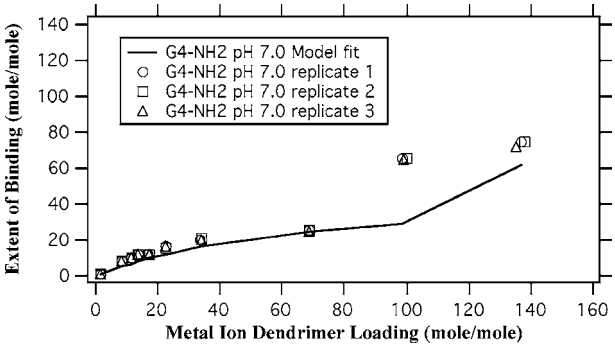

FIGURE 3. Two-site model of Cu(II) uptake by G4-NH_2 PAMAM dendrimer in aqueous solutions: model fit versus measured extent of binding at room temperature and pH 7.0. Data are taken from Diallo et al. (*15*).

to the dendrimers tertiary amine groups at pH 7.0, Diallo et al. (*15*) hypothesized the formation of octahedral complexes of Cu(II) with water molecules trapped inside the G*x*-NH_2 PAMAM dendrimers. They subsequently were able to formulate a two-site thermodynamic model of Cu(II) binding to G*x*-NH_2 PAMAM dendrimers based on (i) the postulated mechanisms of Cu(II) coordination with the dendrimer tertiary amine groups and bound water molecules (*15*) and (ii) Tanford's theory of solute binding to macromolecules in aqueous solutions (*37*). This model expresses the EOB of Cu(II) in aqueous solutions (at neutral pH) of G*x*-NH_2 PAMAM dendrimers as function of the metal ion−dendrimer loading (N_{Cu0}/N_d), the number of dendrimer tertiary amine groups (N_N^d), the number of water molecules bound to the dendrimers (N_{H2O-d}), the metal ion−dendrimer tertiary amine groups coordination number ($CN^d_{Cu(II)-N}$), the metal ion−dendrimer bound water molecules coordination number ($CN^d_{Cu(II)-H2O}$), and the intrinsic association constants of Cu(II) to the dendrimer tertiary amine groups and bound water molecules ($k^d_{Cu(II)-N}$ and $k^d_{Cu(II)-H2O}$). Figure 3 highlights the results of a preliminary evaluation of the model. All the data used to evaluate the model are taken from Diallo et al. (*15*). At low metal ion−dendrimer loadings, the model provides a good fit of the measured EOB of Cu(II) for the G4-NH_2 PAMAM dendrimer. The model also reproduces the increase in the EOB observed at higher metal ion−dendrimer loadings following the first plateau. Note that the two-site model can also be used to estimate the binding constant of Cu(II) [$K^d_{Cu(II)-N} = (N_N^d/k^d_{Cu(II)-N})$] to the tertiary amine groups of a G*x*-NH_2 PAMAM dendrimer. The $K^d_{Cu(II)-N}$ values for the G4-NH_2 and G5-NH_2 EDA core PAMAM dendrimers are respectively equal to 3.15 and 3.78. As shown in Table 3, the binding constants of Cu(II) to the tertiary amine groups of the G*x*-NH_2 PAMAM dendrimers (*15*) are comparable in magnitude to the formation constants of Cu(II)−ammonia complexes (*38*). Ammonia (NH_3) is representative of metal ion chelating agents with saturated N donors (*38*). Table 3 also suggests that the G*x*-NH_2 PAMAM dendrimers will selectively bind Cu(II) over first-row transition metal ions such as Co(II) and Ni(II) and alkaline earth metal ions in wastewater such as Na(I), Ca(II), and Mg(II).

TABLE 3. Formation Constants of Selected Metal Ion−Ammonia Complexes and Estimated Binding Constants of Cu(II) to the Tertiary Amines Groups of EDA Core G*x*-NH2 PAMAM Dendrimers

metal ion	log K_1 (NH_3)[a]	log $K^d_{Cu(II)-N}$ (G4-NH_2)[b]	log $K^d_{Cu(II)-N}$ (G4-NH_2)[c]
Cu(II)	4.04	3.15	3.78
Co(II)	2.10	na[d]	na
Ni(II)	2.70	na	na
Na(I)	−1.1	na	na
Mg(II)	0.23	na	na
Ca(II)	−0.2	na	na

[a] Data are taken from Martell and Hancock (*38*). [b] Estimated using the two-site thermodynamic model of Cu(II) binding to G*x*-NH_2 PAMAM dendrimers at neutral pH developed by Diallo et al. (*15*). [c] The Cu(II) binding capacity of the linear polymers with amine groups were taken from Geckeler and Volchek (*2*). [d] na, not available.

Building upon the results of our fundamental investigations of Cu(II) binding to PAMAM dendrimers (*14*, *15*), we have begun the evaluation and optimization of dendrimer enhanced ultrafiltration (DEUF) as a cost-effective and environmentally acceptable separation process for recovering metal ions such as Cu(II) from aqueous solutions. The dendrimer-enhanced filtration process (Figure 4) is a patented process (*39*) structured around two unit operations: (i) a clean water recovery unit and (ii) a dendrimer recovery unit. In the clean water recovery unit, contaminated water is mixed with a solution of functionalized dendritic polymers [e. g., dendrimers, dendrigfrat polymers, hyperbranched polymers, core−shell tecto(dendrimers), etc.] to carry out the specific reactions of interest (metal ion chelation in this case). Following completion of the reaction, the resulting solution is filtered to recover the clean water. The contaminant-laden dendrimer solutions are subsequently sent to a second filtration unit to recover and recycle the functionalized dendritic polymers (Figure 4). As a proof-of-concept study of this novel water treatment process, we carried out dead-end utrafiltration (UF) experiments to assess the feasibility of using DEUF to recover Cu(II) from aqueous solutions. To gain insight into membrane fouling, we used atomic force microscopy (AFM) to characterize dendrimer sorption onto model UF membranes. The overall results of these experiments suggest that DEUF is a promising process for recovering Cu(II) from aqueous solutions.

Experimental Procedures

Ultrafiltration Experiments. We focused on the evaluation of the commercially available EDA core G*x*-NH_2 PAMAM

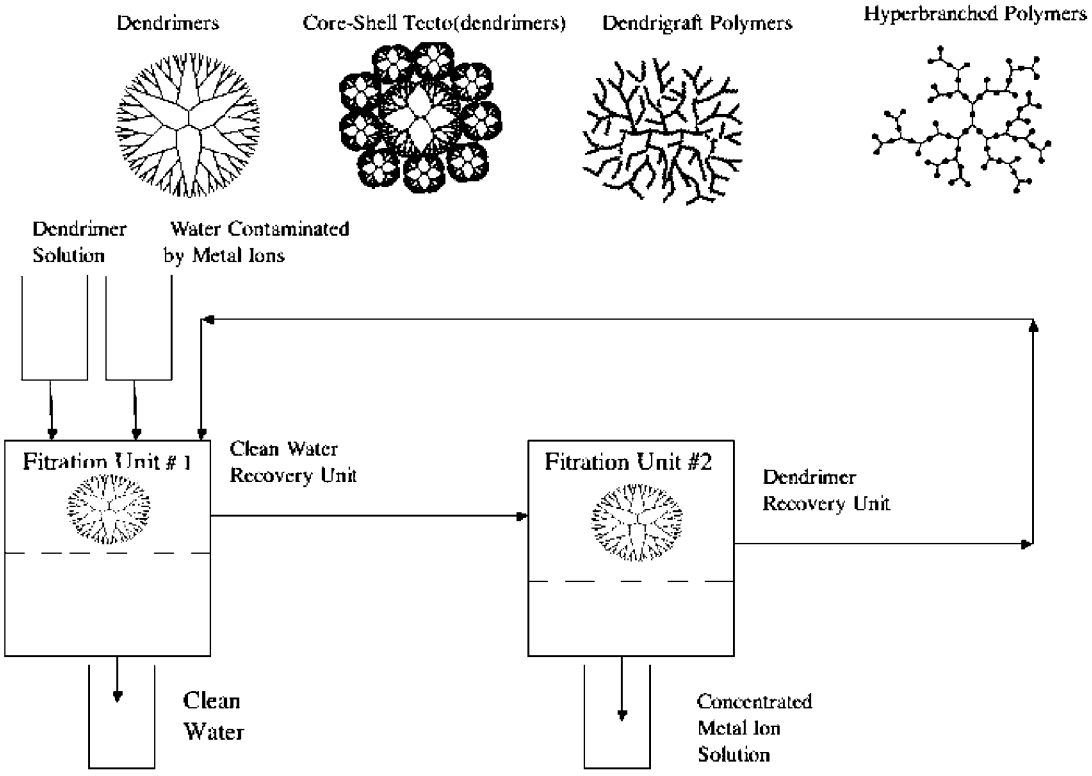

FIGURE 4. Recovery of metal ions from aqueous solutions by dendrimer enhanced ultrafiltration (*39*).

dendrimers (Figure 1). G3-NH_2, G4-NH_2, and G5-NH_2 EDA core PAMAM dendrimers were purchased from Sigma-Aldrich and used as received. Selected physicochemical properties of the PAMAM dendrimers are given in Table 1. Cu(II) was selected as model metal ion for this study. Reagent grade $Cu(NO_3)_2$ from Sigma-Aldrich was used as source of Cu(II). UF experiments were carried out to measure the retention of dendrimers and Cu(II)−dendrimer complexes by model UF membranes. The experiments were performed in a 10-mL stirred cell (Amicon, model 8010) with an effective membrane area of 4. 1 cm^2. A 1-gal stainless steel dispensing pressure vessel (Millipore) was connected to the stirred cell using PVC tubing. The reservoir was also equipped with a pressure gauge and relief valve. Pressure from nitrogen gas was applied to the stirred cell via the reservoir at 450 kPa (65 psi). For each run, the initial volume was 1 L. During each UF experiment, the stirred cell was operated for 4.5 h with permeate collected every 30 min, and flux measurements were taken every 10 min.

Ultracel Amicon YM regenerated cellulose (RC) and PB Biomax polyethersulfone (PES) membranes from Millipore were evaluated in this study. The RC and PES membranes had a diameter of 25 mm with molecular weight cutoff (MWCO) of 5000 Da (5 kDa) and 10 000 Da (10 kDa). For the UF measurements of dendrimer retention in aqueous solutions, the concentrations of the G3-NH_2 (2.42265×10^{-5} mol/L), G4-NH_2 (8.49762×10^{-6} mol/L), and G5-NH_2 (5.31808×10^{-6} mol/L) PAMAM dendrimers were kept constant in all experiments. Dendrimer concentrations in the feed and permeate solutions were measured using a Shimadzu model 1601 UV−visible spectrophotometer at a wavelength of 201 nm. A detailed description of analytical techniques [including HPLC with UV−visible detection] used to characterize the composition and purity of EDA core PAMAM dendrimers is given elsewhere (*15*). For the UF measurements of the retention of metal ion−dendrimer complexes, a Cu(II) concentration of 10 mg/L (1.5738×10^{-4} mol/L) was used in all experiments. The molar ratio of Cu(II) to dendrimer NH_2 groups was also kept constant at 0.2 in all experiments. The Cu(II)−dendrimer solutions were maintained under constant agitation for 1 h in the dispensing pressure vessel following adjustment of their pH with concentrated HCl or NaOH. The pH of aqueous solutions of PAMAM dendrimers and their complexes with Cu(II) can be controlled within 0.1−0.2 pH unit by addition of concentrated NaOH or HCl (*15*). The concentrations of metal ion in the feed and permeate were determined by atomic absorption spectrophotometry (*14, 15*). Solute retention (R) was expressed as

$$R = \left(1 - \frac{C_p}{C_f}\right) \times 100 \quad (1)$$

where C_p and C_f are respectively the concentration of solute [i.e., dendrimer and Cu(II)] in the permeate and feed. The permeate flux J_p (L h^{-1} m^{-2}) and normalized permeate flux (J_{pn}) were expressed as

$$J_p = \frac{Q_p}{A_{UF}} \quad (2)$$

$$J_{pn} = \frac{J_p}{J_{po}} \quad (3)$$

where Q_p is the permeate flow rate (L h^{-1}), A_{UF} (m^2) is the effective area of the UF membrane, and J_{po} (L h^{-1} m^{-2}) is the initial permeate flux through the clean membranes.

AFM Characterization Studies. AFM was employed to characterize the interactions of selected EDA core G*x*-NH_2 PAMAM dendrimers and UF membranes evaluated in this study. Each UF membrane was mounted on a perforated aluminum sheet and stored overnight in a desiccators following exposure to a dendrimer aqueous solution as previously described. Tapping mode AFM experiments were carried out using a Model Dimension 3100 AFM from Digital Instruments. All AFM images were acquired at room temperature using etched silicon probes with a spring constant of 20−100 N/m and a tip radius of 5−10 nm. The topographic

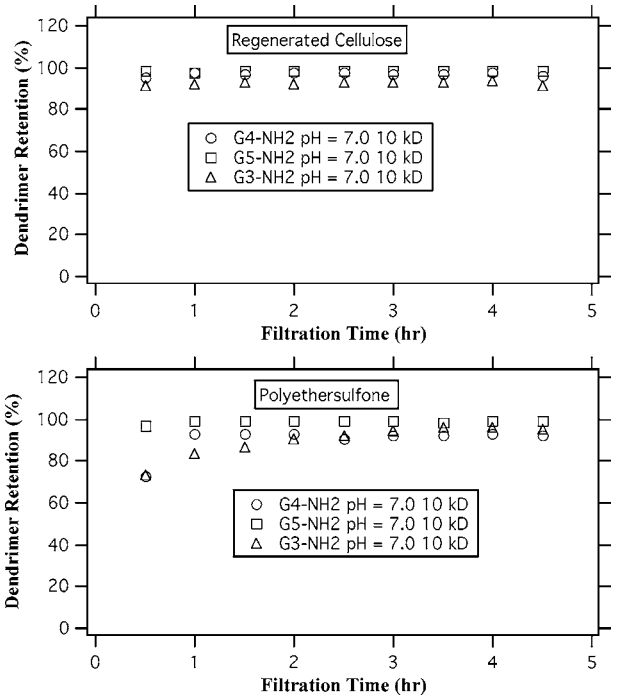

FIGURE 5. Retention of EDA core G*x*-NH_2 PAMAM dendrimers in aqueous solutions as a function of solution pH and membrane chemistry.

and phase images of the clean and exposed UF membranes were acquired simultaneously using a probe resonance frequency of ~300 kHz, a scan rate of 1 Hz, a free-oscillation amplitude (A_o) of 60 nm ± 5 nm, and a set point to free amplitude ratio (rsp) of 0.50−0.75.

Results and Discussion

Retention of EDA Core G*x*-NH_2 PAMAM Dendrimers by UF Membranes. Figure 5 highlights the effects of dendrimer generation and membrane chemistry on the retention of EDA core G*x*-NH_2 PAMAM dendrimers in aqueous solutions at pH 7.0 and room temperature. The retentions of the G5-NH_2 PAMAM dendrimer by the 10 kDa RC and PES membrane are ≥97% in all cases. Such high retention values are expected for the G5-NH_2 EDA core PAMAM dendrimer, a globular macromolecule with a low polydispersity and a molar mass of 28 826 Da (Table 1). For the most part, retentions greater than 90% are also observed for the G4-NH_2 PAMAM dendrimer (Figure 5). This dendrimer is also globular in shape and has very low polydispersity with a molar mass (14 215 Da) greater than the MWCO of the 10 kDa RC and PES membranes (Table 1). Presently, we have no clear explanation for the initial low retention (≈73%) of this dendrimer by the 10 kDa PES membrane. Possible explanation includes measurement errors or the presence of impurities such as unreacted EDA and other lower molar mass reaction byproducts in the G4-NH_2 PAMAM dendrimer sample (*15*).

Not surprisingly, Figure 5 also shows that the retentions of the G3-NH_2 EDA core PAMAM dendrimer are lower than those of the higher generation dendrimers. This dendrimer has the lowest molar mass (Table 1). Note that for both membranes there is a significant retention of the G3-NH_2 dendrimer even though the MWCO of the membrane is 45% larger than the dendrimer molar mass (6906 Da). In fact, the retention of the G3-NH_2 dendrimer by the 10 kDa RC membrane (Figure 5) is comparable to that of a linear polyethyleneimine (PEI) polymer with an average molar mass of 50−60 kDa (*4*). For UF membranes, the MWCO is usually defined as the molar mass of a globular protein with 90%

Figure 6:

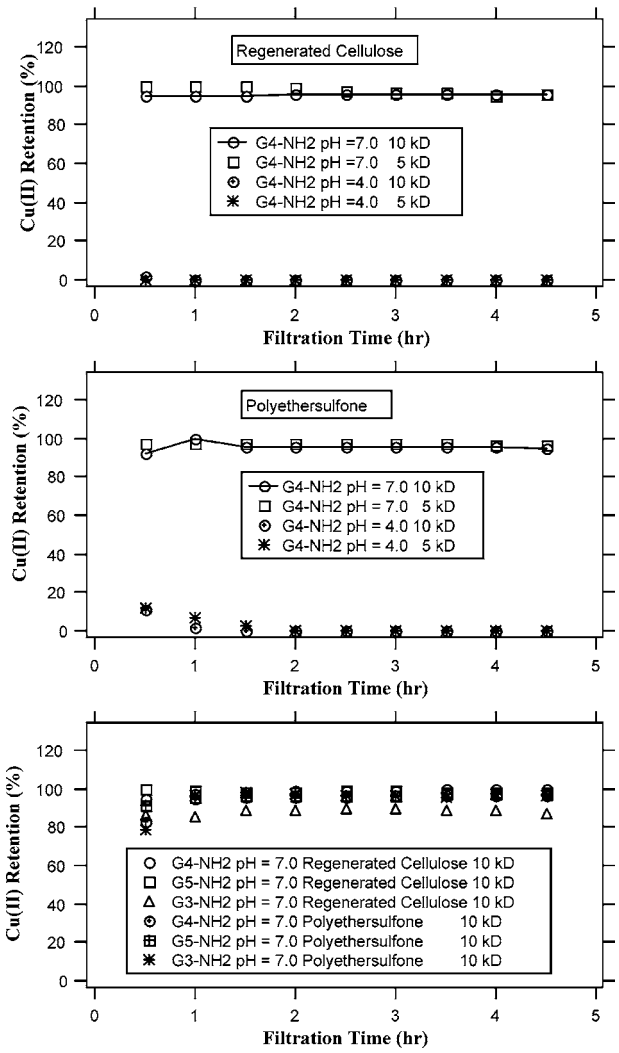

FIGURE 6. Cu(II) retention in aqueous solutions of EDA core G*x*-NH_2 PAMAM dendrimers as a function of solution pH, membrane chemistry, and molecular weight cutoff.

retention. Because dendritic polymers can be described as hybrids between polymer chains and colloidal particles (*40, 41*), the use of the MWCO as indicator of dendrimer retention by UF membranes might not be adequate. Table 1 gives the radius of gyration (R_G) and hydrodynamic radius (R_H) of each EDA core G*x*-NH_2 PAMAM dendrimer evaluated in this study. R_G provides a measure of the size of a particle/macromolecule regardless of its shape (*42, 43*). Conversely, R_H gives the size of an "equivalent" spherical particle/macromolecule (*44*). The R_G and R_H of the PAMAM dendrimers were estimated from small angle neutron scattering experiments (*45*) and dilute solution viscosity measurements (*45*), respectively. They are comparable in magnitude to the mean pore surface diameters (1.93−3.14 nm) of a series of UF membranes (1−10 kDa MWCO) that was recently characterized by Bowen and Doneva (*46*). Whereas the molar mass of each G*x*-NH_2 PAMAM dendrimer increases by a factor of 2 at each generation, Table 1 shows that the corresponding radii of gyration and hydrodynamic radii increase linearly with dendrimer generation. Table 1 also shows no significant differences between the R_G and R_H of each G*x*-NH_2 PAMAM dendrimer. We believe the slightly higher R_H values could be attributed for the most part to dendrimer hydration. Because the differences in the retentions of the EDA core G*x*-NH_2

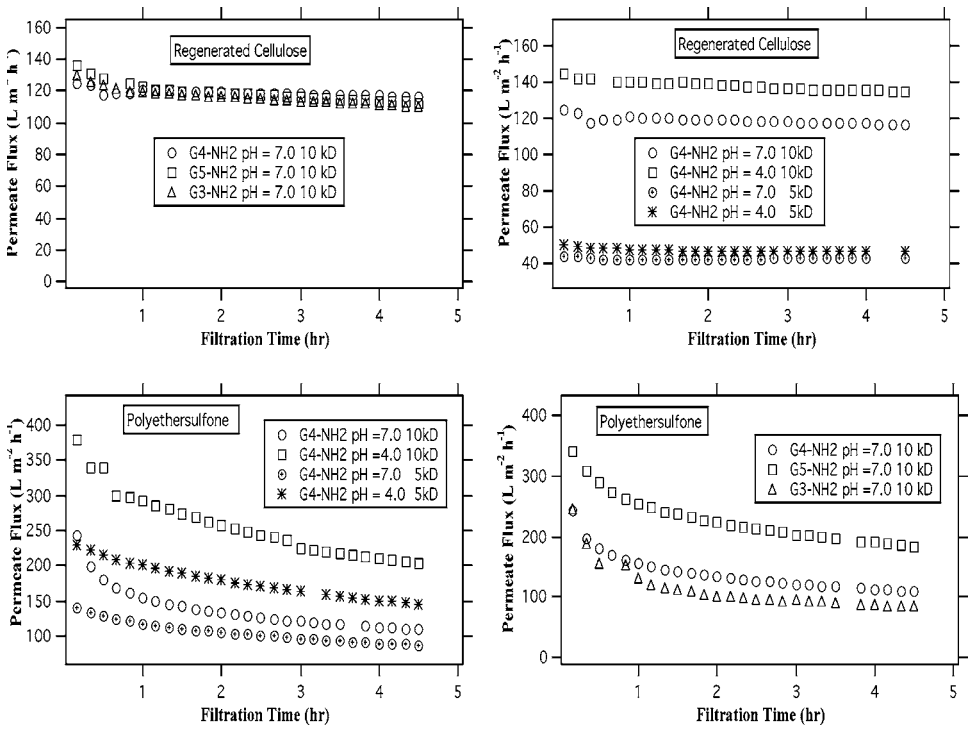

FIGURE 7. Permeate flux in aqueous solutions of Cu(II) + EDA core G*x*-NH_2 PAMAM dendrimer as a function of solution pH, membrane chemistry, and molecular weight cutoff.

PAMAM dendrimers are (for the most part) comparable to the differences between their radii of gyration and hydrodynamic diameter, the R_G/R_H appears to be a better indicator of dendrimer retention by UF membranes in aqueous solutions. The overall results of the measurements of dendrimer retention by the 10 kDa RC and PES membranes at pH 7.0 suggest that dendrimers such the G*x*-NH_2 EDA core PAMAM have much less tendency to pass through the pores of UF membranes than linear polymers of similar molar mass because of their much smaller polydispersity and persistent globular shapes in aqueous solutions over a broad range of solution pH and background electrolyte concentration (*11*−*13*).

Retention of Cu(II)−Dendrimer Complexes by the UF Membranes. Figure 6 highlights the effects of solution pH, membrane chemistry, and MWCO on the retention of aqueous complexes of Cu(II) with a G4-NH_2 EDA core PAMAM dendrimer at room temperature. A Cu(II) concentration of 10 mg/L (0.00016 mol/L) was used in all experiments. The molar ratio of Cu(II) to dendrimer NH_2 groups was also kept constant at 0.2 to ensure that all the Cu(II) ions will be bound to the tertiary amine groups of the G*x*-NH_2 PAMAM dendrimers at pH 7.0 (*15*). As shown in Figure 6, 95−100% of the complexes of Cu(II) with the G4-NH_2 PAMAM dendrimer are retained by the RC membranes at pH 7.0. The PES membranes also retain 92−100% of the Cu(II)−dendrimer complexes at pH 7.0. These results are consistent with the measurements of dendrimer retention (Figure 5) and metal ion binding measurements, which show that 100% of the Cu(II) ions are bound to the G4-NH_2 PAMAM dendrimer at pH 7.0 and Cu(II) dendrimer terminal NH_2 groups molar ratio of 0.2. Consistent with the results of the metal ion binding measurements and dendrimer extent of protonation (*15*), no retention of Cu(II)−dendrimer complexes by the RC membranes occurs at pH 4.0 (Figure 6). However, a small retention of Cu(II) (∼10%) is initially observed for both PES membranes at pH 4.0. Presently, we have no clear explanation for this result. Possible explanations include measurement errors or metal ion sorption onto the PES membranes. Additional experiments are currently underway to address this issue.

Figure 6 illustrates the effects of dendrimer generation on the retention of Cu(II)−dendrimer complexes by the 10 kDa membranes at pH 7.0. Here again, the observed retention values are consistent with the results of the dendrimer retention measurements (Figure 5). Not surprisingly, higher retention values are observed for the complexes of Cu(II) with the G5-NH_2 PAMAM dendrimer. Conversely, smaller retention values for the Cu(II)−dendrimer complexes are observed with the G3-NH_2 PAMAM dendrimer (Figure 6). Note that for both membranes, Figure 6 shows significant retentions of Cu(II) complexes with the G3-NH_2 dendrimer [86−89% for the 10 kDa RC membrane and 80−97% for the 10 kDa PES membrane] even though the MWCO of each membrane is 45% larger than the dendrimer molar mass. These results also suggest that the MWCO of a UF membrane might not be an adequate indicator of the retention of Cu(II) + dendrimer complexes by UF membranes in aqueous solutions.

Permeate Fluxes through the UF Membranes. Fouling is a major limiting factor to the use of membrane-based processes in environmental and industrial separations (*47*, *48*). A characteristic signature of membrane fouling is a reduction in permeate flux through a membrane during filtration. We measured the permeate fluxes of aqueous solutions of Cu(II) complexes with G*x*-NH_2 PAMAM dendrimers through RC and PES membranes at pH 7.0 and pH 4.0. In these experiments, the Cu(II) concentration (1.5738×10^{-4} mol/L) and molar ratio of Cu(II) to dendrimer NH_2 groups (0.2) were also kept constant. Figure 7 shows the permeate fluxes through the RC and PES membranes. For the 10 kDa RC membrane at pH 7.0, the permeate flux shows little change over the course of the filtration varying from 124.0 to 116.0 L m^{-2} h^{-1}. A similar behavior is also observed at pH 4.0. However, in this case, the permeate fluxes are approximately 16% higher. The permeate fluxes through the 5 kDa RC membranes also exhibit little variation (49.0−43.0 L m^{-2} h^{-1}) during the course of the filtration at pH 7.0 and

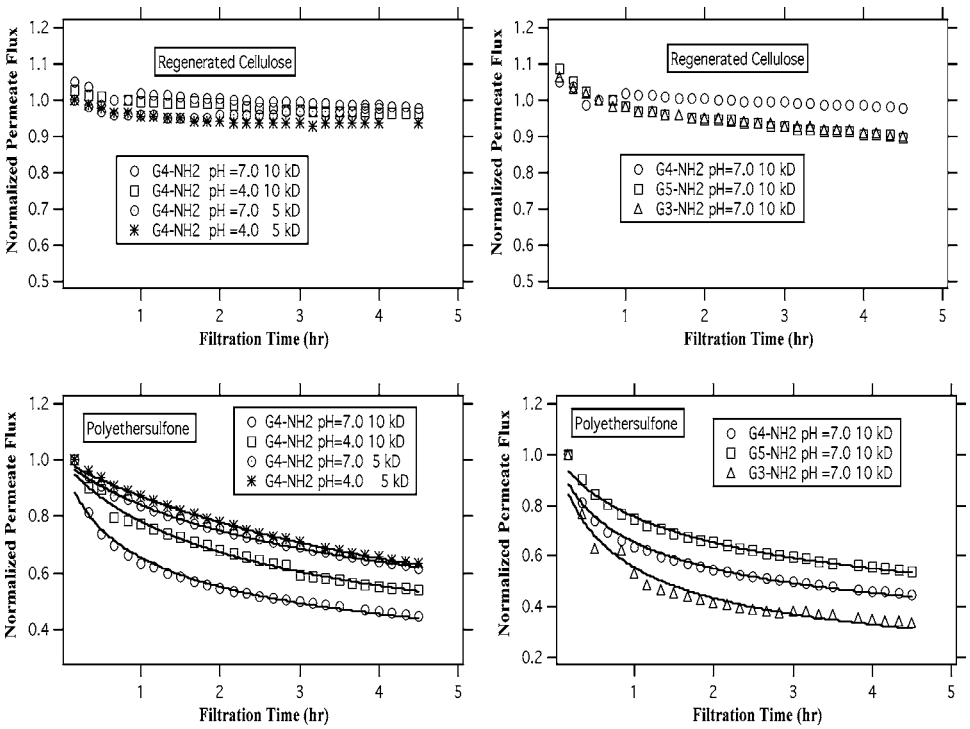

FIGURE 8. Normalized permeate flux in aqueous solutions of Cu(II) + EDA core G*x*-NH_2 PAMAM dendrimer as a function of solution pH, membrane chemistry, and molecular weight cutoff.

pH 4.0 (Figure 7). Figure 7 also shows that dendrimer generation does not significantly affect the permeate flux through the 10 kDa RC membrane. This sharply contrasts the significant decline of permeate flux observed for the 5 and 10 kDa PES membranes (Figure 7). Although the initial permeate fluxes are much larger for the PES membranes, significant flux declines (45−63%) occur during the filtration of aqueous solutions of Cu(II) complexes with the G4-NH_2 PAMAM dendrimer at pH 7.0 and pH 4.0 (Figure 7). In this case, we also observe a significant impact of dendrimer generation on the permeate flux of aqueous solutions of Cu(II)−dendrimer complexes through the 10 kDa PES membranes at pH 7.0. Figure 8 shows a decline in the normalized permeate fluxes for both the RC and PES membranes during the filtration of aqueous solutions of Cu(II) complexes with G*x*-NH_2 PAMAM dendrimer at pH 7.0. For the 5 and 10 kDa RC membranes, a small decrease in the relative permeate flux (7−18%) is observed. However, this decrease (46−81%) is much larger for the PES membranes. At pH 4.0, a significant decrease in permeate flux (13−68%) is also observed for the PES membranes. These results suggest that the PES membranes are more susceptible to fouling by the aqueous solutions of G*x*-NH_2 PAMAM dendrimer + Cu(II) than the corresponding RC membranes.

The mechanisms of fouling of UF membranes are not well understood. For organic macromolecules such as proteins, linear polymers, and humic acids, membrane fouling may be caused by (i) concentration polarization resulting from solute accumulation near a membrane surface, (ii) pore blockage by solute sorption onto the surface of a membrane or within its pores, and (iii) formation of a cake layer by sorption/deposition of solutes on a membrane surface (*47, 48*). To learn more about the fouling of the RC and PS membranes by EDA core G*x*-NH_2 PAMAM dendrimers, we used the data analysis software IGOR Pro Version 4.0 from WaveMetrics, Inc. (*49*) to fit the normalized permeate fluxes to two phenomenological models of membrane fouling (Figure 8). The first model is a pore blockage model that expresses the decline in the normalized permeate flux as an exponential decay function (*47, 48*). This model did not provide a good fit of the data (results not shown). The second model expresses the decline in the normalized permeate flux as a power-law function (*47, 48*):

$$J_{pn} = (1 + kt)^{-n} \quad (4)$$

where k (h^{-1}) is a filtration rate constant and n is a dimensionless exponent. As shown in Figure 8 and Table 4, this model provides a very good fit of the normalized permeate flux for the all the PES membranes. For the G4-NH_2 PAMAM dendrimer, the estimated values of n for the 10 kDa PES membranes are 0.31 ± 0.03 at pH 7.0 and 0.39 ± 0.03 at pH 4.0 (Table 4). For the 5 kDa PES membrane, the n values are equal to 0.36 ± 0.02 at pH 7.0 and 0.63 ± 0.05 at pH 4.0 (Table 4). The n values for the G3-NH_2 and G5-NH_2 PAMAM dendrimers membranes are equal to 0.45 ± 0.05 and 0.30 ± 0.02, respectively, for the10 kDa PES membranes at pH 7.0. For dead-end ultrafiltration, Zeeman and Zydney (*47*) and Kilduff et al. (*48*) have shown that the decline in permeate flux can be described by a pore constriction model when $n \sim 2$. This model assumes that the rate of change in the membrane pore volume is proportional to the rate of

TABLE 4. Fitted Model Parameters for Normalized Permeate Flux of Aqueous Solutions of EDA Core G*x*-NH_2 PAMAM Dendrimers + Cu(II) through Polyethersulfone Membranes

dendrimer	membrane MWCO (kDa)	pH	k (h^{-1})[a]	n[a]	χ^2 [b]
G4-NH_2	10	7.0	2.98 ± 0.58	0.31 ± 0.03	0.016
G4-NH_2	10	4.0	0.86 ± 0.13	0.39 ± 0.03	0.007
G4-NH_2	5	7.0	0.62 ± 0.06	0.36 ± 0.02	0.001
G4-NH_2	5	4.0	0.24 ± 0.05	0.63 ± 0.05	0.001
G5-NH_2	10	7.0	1.53 ± 0.21	0.30 ± 0.02	0.016
G3-NH_2	10	7.0	2.74 ± 0.75	0.45 ± 0.05	0.037

[a] k and n are determined by fitting the measured relative permeate fluxes to eq 4. [b] Goodness-of-fit parameter. $\chi^2 = \sum_i (y - y_i/\sigma_i)$; where y is the fitted value, y_i is the measured value, and σ_i is the estimated standard deviation for y_i (*49*).

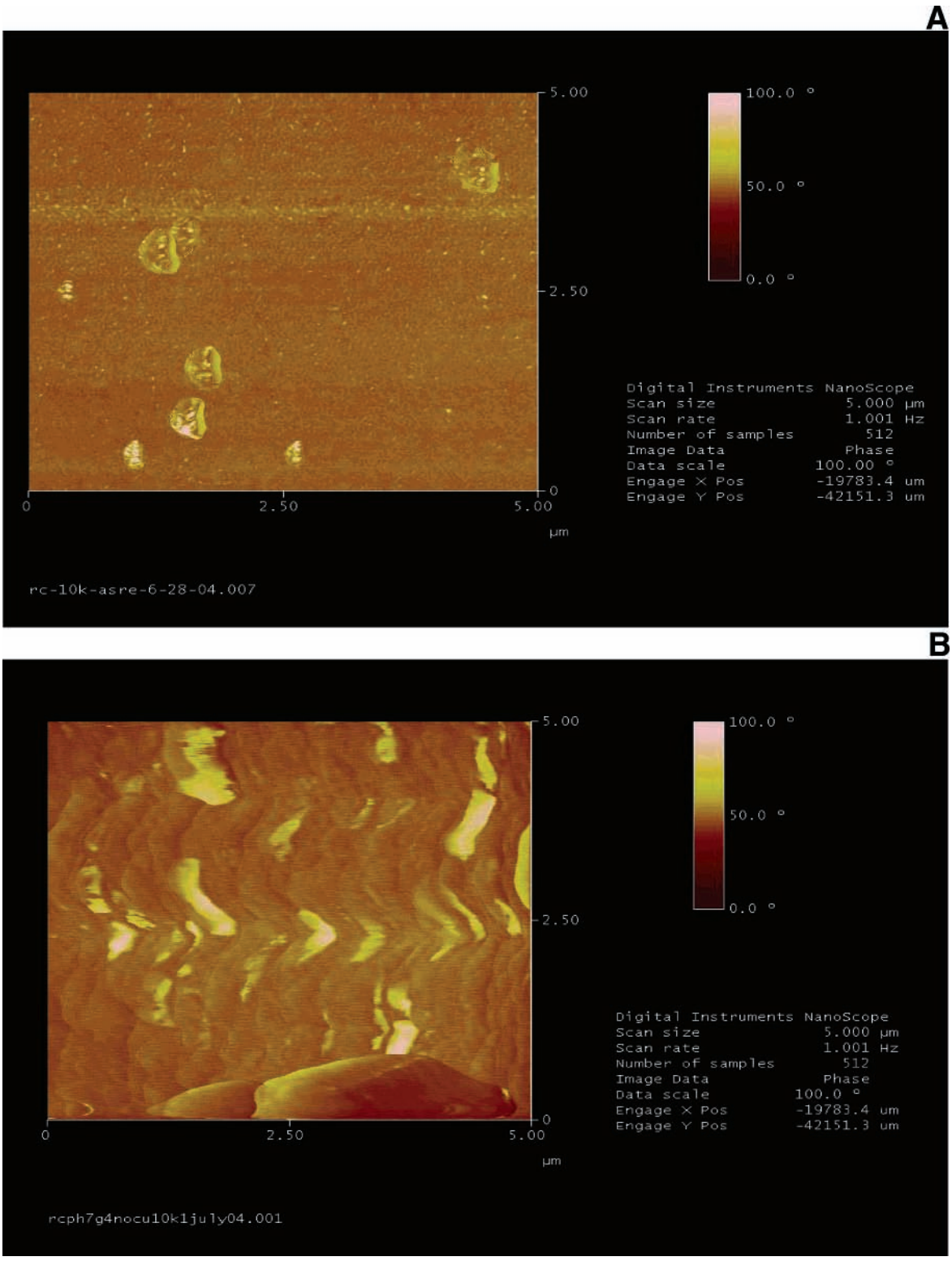

FIGURE 9. AFM images of clean and fouled regenerated cellulose membranes. The scan area is 5 μm $\times$ 5 μm. The fouled membrane was exposed to an aqueous solution of 1.2295 $\times$ 10^{-5} mol/L G4-NH_2 EDA core PAMAM at pH 7.0 for 4.5 h as described in the Experimental Procedures.

particle convection to the membrane surface. When $n \sim 0.5$, the decline in permeate flux in a dead-end ultrafiltration process can be described by a cake filtration model (*47, 48*). This model attributes the loss of permeate flux to particle deposition on the membrane surface. On the basis of the estimated n values given in Table 4, the sorption and deposition of dendrimer + Cu(II) complexes onto the membrane surfaces appears to be a plausible fouling mechanism for the PES membranes. We also believe that the small decline in the normalized permeate fluxes (7−18%) through the 5 and 10 K RC membranes (Figure 8) could also be attributed to the sorption of dendrimer−Cu(II) complexes onto the membrane surfaces.

AFM Characterization Experiments. To gain insight into the relationship between dendrimer sorption and membrane fouling, we used AFM to characterize RC and PES membranes

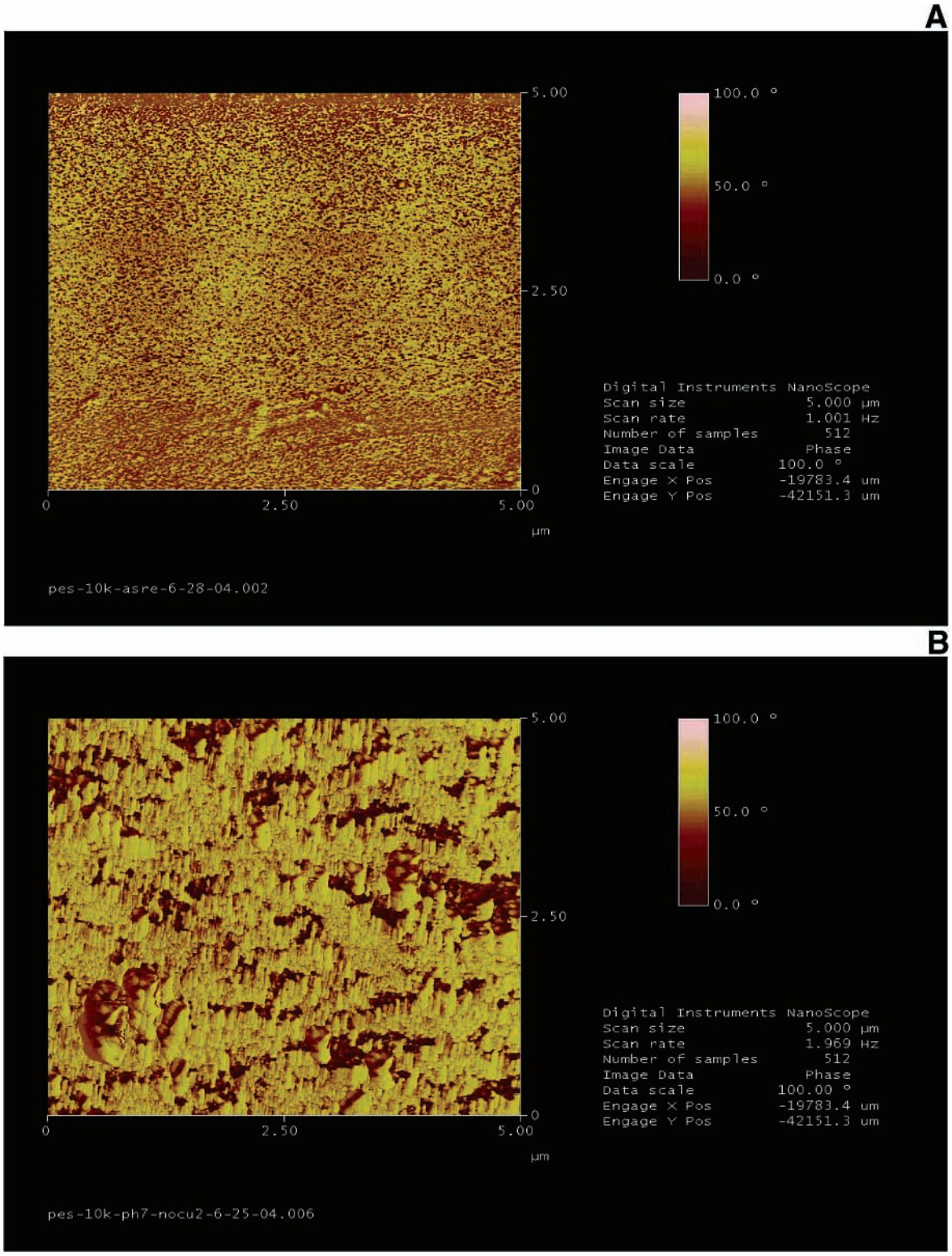

FIGURE 10. AFM images of clean and fouled polyethersulfone membranes. The scan area is 5 μm × 5 μm. The fouled membrane was exposed to an aqueous solution of 1.2295 × 10^{-5} mol/L G4-NH_2 EDA core PAMAM at pH 7.0 for 4.5 h as described in the Experimental Procedures.

that have been exposed to a G4-NH_2 PAMAM dendrimer at pH 7.0 during the filtration experiments. AFM has emerged as a powerful tool for charactering filtration membranes (*46, 47, 50*−*54*). AFM has also successfully been used to characterize G*x*-NH_2 PAMAM dendrimers adsorbed onto solid surfaces (*55*−*57*). Figures 9 and 10 show AFM images of clean and fouled 10 kDa RC and PES membranes. A scan area of 5 μm × 5 μm was used in all the AFM experiments. The fouled membranes were exposed to aqueous solutions of 1.2295 × 10^{-5} mol/L G4-NH_2 EDA core PAMAM at pH 7.0 for 4.5 h as described in the Experimental Procedures. The AFM images were subsequently analyzed (*58*) to determine the roughness parameter (RMS), the mean roughness (R_a), and the maximum height (R_{max}) along two different sections. The results of this analysis are given in Table 5 and Supporting Information. To the best of our knowledge, these are the first

TABLE 5. Section Analysis of AFM Images of Clean and Fouled Regenerated Cellulose (RC) and Polyethersulfone (PES) Ultrafiltration Membranes

membrane	status	RMS (nm)[a]	R_a (nm)[b]	R_{max} (nm)[c]
10 kDa RC	clean[d]	4.63−3.45	2.09−1.73	51.48−36.58
10 kDa RC	fouled[e]	9.20−6.56	5.46−3.32	55.23−49.17
10 kDa PES	clean[d]	14.96−13.07	11.76−9.28	51.75−47.56
10 kDa PES	fouled[e]	14.07−14.22	9.90−10.25	61.66−65.86

[a] RMS is the standard deviation $\sigma = (\sum_i (Z_i - Z_{ave})/N$ (*58*); where Z_i is the height at point *i*, Z_{ave} is the average height, and *N* is the number of points *i* between the reference markers. The reference markers are the red triangles of the AFM images shown in Figures SI1−SI4 in the Supporting Information. [b] R_a is the "mean roughness". $R_a = 1/L \int_0^L |f(x)|$ d*x* (*58*), where *L* is the length of the roughness curve and $f(x)$ is the roughness curve relative to the center line [see the Analysis of Figures SI1−SI4 section in the Supporting Information]. [c] R_{max} is the "maximum height" (*58*). It is the difference in height between the highest and lowest points on the cross-sectional profile relative to the center line [see the Analysis of Figures SI1−SI4 section in the Supporting Information]. [d] As received from Millipore. [e] Exposed to a 1.2295×10^{-5} mol/L aqueous solution of G4-NH_2 PAMAM dendrimer in a 10-mL dead-end stirred cell (Amicon, model 8010) during 4.5 h as described in the Experimental Procedures section.

published AFM images of G*x*-NH_2 PAMAM dendrimers sorbed onto the surface of UF membranes. Except for the presence of a few "rough" spots, the clean 10 kDa RC membrane exhibits a smooth and uniform skin. Conversely, the PES membrane exhibits a dense, tightly, packed and grainy structure characteristics of membranes with nodular skin morphology (*47*). The RMS and R_a of the clean PES membrane are significant larger than those of the clean RC membrane (Table 5). As shown in Figure 9, only a small fraction of the fouled RC membrane is covered by the sorbed G4-NH_2 PAMAM dendrimers. Although we were not able to fully resolve the location of individual dendrimer molecules, most of the sorbed dendrimer molecules appear to cluster around the "rough" spots of the RC membrane surface (Figure 9) thereby suggesting that dendrimer sorption in this case is a nonspecific process primary driven by membrane surface roughness (*50, 53*). This sharply contrasts the extensive coverage of the PES membrane surface by sorbed dendrimers (Figure 10). Here we believe that dendrimer sorption on the PES surface is mediated by electrostatic attractions between the protonated terminal NH_2 groups of the G4-NH_2 PAMAM dendrimer (Figure 3) and the negatively charged PES membranes at pH 7.0. The overall results of the AFM experiments suggest that there is a significant correlation between the extent of dendrimer sorption and membrane fouling. Additional experiments are underway to further assess this correlation.

Environmental Implications. As stated in the introductory section, polymer enhanced ultrafiltration (PEUF) has emerged as a promising process for recovering metal ions from aqueous solutions (*2*−*10*). The efficiency of PEUF-based processes for treatment of water contaminated by metal ions will depend on several factors including: (i) polymer binding capacity and selectivity toward the targeted metal ions; (ii) polymer molar mass and responsiveness to stimuli such as solution pH; (iii) polymer sorption tendency onto UF membranes; and (iv) polymer stability and toxicity. An ideal polymer for PEUF treatment of water contaminated by metal ions should be highly soluble in water and have a high binding capacity/selectivity toward the targeted metal ions along with a low sorption tendency toward UF membranes. Its molar mass should be high enough to ensure complete retention of the metal ion-polymer complexes by UF membranes without significant polymer leakage and decrease in permeate flux. The metal ion binding capacity of an ideal polymer for PEUF should also exhibit sensitivity to stimuli such as solution pH over a range broad enough to allow efficient recovery and recycling of the polymer by a simple change of solution pH. An ideal polymer for PEUF should also be nontoxic and stable with a long life cycle to minimize polymer consumption.

On a mass basis, the Cu(II) binding capacities of the G*x*-NH_2 PAMAM dendrimers are much larger and more sensitive to solution pH (Table 2) than those of linear polymers with amine groups that have been used in previous PEUF studies (*2*). Table 3 shows that Na(I), Ca(II), and Mg(II) have very low binding affinity toward ligands with N donors such as NH_3. Thus, the high concentrations of Na(I), Ca(II), and Mg(II) found in most industrial wastewater streams are not expected to have a significant effect on the Cu(II) binding capacity and selectivity of EDA core G*x*-NH_2 PAMAM dendrimers. As shown in Figure 6, separation of the dendrimer−Cu(II) complexes from solutions can simply be achieved by ultrafiltration. The metal ion laden dendrimers can also be regenerated by decreasing the solution pH to 4.0 (Figure 6). Dendritic macromolecules such the G*x*-NH_2 EDA core PAMAM dendrimers have also much less tendency to pass through the pores of UF membranes (Figure 5) than linear polymers of similar chemistry and molar mass (*2, 4*) because of their much smaller polydispersity and globular shape (*11*−*13*). They have also a very low tendency to foul the commercially available RC membranes evaluated in this study (Figures 7−9). Whereas the intrinsic viscosity of a linear polymer increases with its molar mass, that of a dendrimer decreases as it adopts a molar globular shape at higher generations (*12, 13*). Because of this, dendrimers have a much smaller intrinsic viscosity than linear polymers with similar molar mass (*12, 13*). Thus, comparatively smaller operating pressure, energy consumption, and loss of ligands by shear-induced mechanical breakdown could be achieved with dendrimers in tangential/cross-flow UF systems typically used to recover metal ions from contaminated water (*2*). These unique properties of the G*x*-NH_2 EDA core PAMAM dendrimers along with their low toxicity (*59*) make dendrimer-enhanced ultrafiltration (Figure 4) a particularly attractive process for recovering metal ions such as Cu(II) from contaminated water. Additional experiments are underway to optimize DEUF as a cost-effective and environmentally acceptable process for recovering metal ions from industrial wastewater solutions.

Acknowledgments

The core funding for this work was provided to Howard University and the California Institute of Technology by the National Science Foundation (NSF Grants CTS-0086727 and CTS-0329436) and the U.S. Environmental Protection Agency (NCER STAR Grant R829626). Partial funding for this research was also provided to Howard University by the Department of Energy (Cooperative Agreement EW15254), the W. M. Keck Foundation, and the NSF Sponsored Cornell University Nanobiotechnology Center. This center is funded by the STC Program of the National Science Foundation under Agreement ECS-9876771. We thank Ms. Sa'Nia Carasquero (graduate student in chemical engineering), Mr. Kwesi Falconer (graduate student in environmental engineering), and Mr. Kori Flowers (undergraduate student in civil engineering) of Howard University School of Engineering for their assistance with the ultrafiltration experiments.

Supporting Information Available

AFM images with section analysis data of clean and fouled 10 kDa RC and PES membranes. This material is available free of charge via the Internet at http://pubs.acs.org.

Literature Cited

(1) Stumm, W.; Morgan, J. J. *Aquatic Chemistry. Chemical Equilibria and Rates in Natural Waters*; John Wiley & Sons: New York, 1996.

(2) Geckeler, K. E.; Volcheck. K. Removal of hazardous substances from water using ultrafiltration in conjunction with soluble polymers. *Environ. Sci. Technol.* **1996**, *30*, 725−734.
(3) Spivakov, B. Y.; Geckeler, K. E.; Bayer, E. Liquid-phase polymer-based retention—the separation of metals by ultrafiltration on polychelatogens. *Nature* **1985**, *315*, 313−315.
(4) Juang, R.; Chen, M. Removal of copper(II) chelates of EDTA and NTA from dilute aqueous solutions by membrane filtration. *Ind. Eng. Chem. Res.* **1997**, *36*, 179−186.
(5) Muslehiddinoglu J.; Uludag, Y.; Ozbelge, H. O.; Yilmaz, L. Effect of operating parameters on selective separation of heavy metals from binary mixtures via polymer enhanced ultrafiltration. *J. Membr. Sci* **1998**, *140*, 251−266.
(6) Juang R. S.; Chiou, C. H. Ultrafiltration rejection of dissolved ions using various weakly basic water-soluble polymers. *J. Membr. Sci* **2000**, *177*, 207−214.
(7) Sanli, O.; Asman, G. Removal of Fe(III) ions from dilute aqueous solutions by alginic acid-enhanced ultrafiltration. *J. Appl. Polym. Sci.* **2000**, *77*, 1096−1101.
(8) Canizares, P.; Perez, A.; Camarillo, R. Recovery of heavy metals by means of ultrafiltration with water-soluble polymers: calculation of design parameters. *Desalination* **2002**, *144*, 279−285.
(9) Llorens, J.; Pujola, M.; Sabate, J. Separation of cadmium from aqueous streams by polymer enhanced ultrafiltration: a two-phase model for complexation. *J. Membr. Sci*. **2004**, *239*, 173−181.
(10) Kryvoruchko, A. P.; Yu, L.; Atamanenko, I. D.; Kornilovich, B. Y. Ultrafiltration removal of U(VI) from contaminated water. *Desalination* **2004**, *162*, 229−236.
(11) Newkome, G. R.; Moorefield, C. N.; Vogtle, F. *Dendritic Molecules. Concepts-Syntheses-Perspectives*; VCH: New York, 1996.
(12) Fréchet, J. M. J., Tomalia, D. A., Eds. *Dendrimers and Other Dendritic Polymers*; Wiley and Sons: New York, 2001.
(13) Bosman, A. W.; Janssen, H. M.; Meijer, E. W. About dendrimers: structure, physical properties and applications. *Chem. Rev*. **1999**, *99*, 1665−1668.
(14) Diallo, M. S.; Balogh, L.; Shafagati, A.; Johnson, J. H., Jr.; Goddard, W. A., III; Tomalia, D. Poly(amidoamine) dendrimers: a new class of high capacity chelating agents for Cu(II) ions. *Environ. Sci. Technol*. **1999**, *33*, 820−824.
(15) Diallo, M. S.; Christie, S.; Swaminathan, P.; Balogh, L.; Shi, X.; Um, W.; Papelis, C.; Goddard, W. A., III; Johnson, J. H., Jr. Dendritic chelating agents. 1. Cu(II) binding to ethylene diamine core poly(amidoamine) dendrimers in aqueous solutions. *Langmuir* **2004**, *20*, 2640−2651**.**
(16) Ottaviani, M. F.; Montali, F.; Turro, N. J.; Tomalia, D. A. Characterization of starburst dendrimers by the EPR technique. 1. Copper-complexes in water solution. *J. Am. Chem. Soc.* **1994**, *116*, 661−671.
(17) Ottaviani, M. F.; Montalti, F.; Turro, N. J.; Tomalia, D. A. Characterization of starburst dendrimers by the EPR technique. Copper(II) ions binding full-generation dendrimers. *J. Phys. Chem*. B. **1997**, *101*, 158−166.
(18) Zhou, L.; Russell D.; H.; Zhao, M. Q.; Crooks R. M. Characterization of poly(amidoamine) dendrimers and their complexes with Cu^{2+} by matrix-assisted laser desorption ionization mass spectrometry. *Macromolecules* **2001**, *34*, 3567−3573.
(19) Ottaviani, M. F.; Montali, F.; Romanelli, M.; Turro, N. J.; Tomalia, D. A. Characterization of starburst dendrimers by EPR. 4. Mn-(II) as a probe of interphase properties. *J. Phys. Chem*. **1996**, *100*, 11033−11042.
(20) Bosman, A. W.; Schemming, A. P. H. J.; Janssen, R. A. J.; Meijer, E. W. Well-defined metallodendrimers by site-specific complexation. *Chem/Ber/Recl.* **1997**, *130*, 725−728.
(21) Vassilev, K.; Ford, W. T. J. Poly(propylene imine) dendrimer complexes of Cu(II), Zn(II), and Co(III) as catalysts of hydrolysis of *p*-nitrophenyl diphenyl phosphate. *J. Polym. Sci. Part A* **1999**, *37*, 2727−2736.
(22) Cohen, S. M.; Petoud, S.; Raymond, K. N. Synthesis and metal binding properties of salicylate-, catecholate-, and hydroxypyridinonate-functionalized dendrimers. *Chem. Eur. J*. **2001**, *7*, 272−279.
(23) Kobayashi, H.; Kawamoto, S.; Saga, T.; Sato, N.; Hiraga, A.; Konishi, J.; Togashi, K.; Brechbiel, M. W. Micro-MR angiography of normal and intratumoral vessels in mice using dedicated intravascular MR contrast agents with high generation of polyamidoamine dendrimer core: reference to pharmacokinetic properties of dendrimer-based MR contrast agents. *Magn. Reson. Imaging* **2001**, *14*, 705−713.
(24) Kobayashi, H.; Kawamoto, S.; Jo, S. K.; Bryant, H. L.; Brechbiel, M. W.; Star, R. A. Macromolecular MRI contrast agents with small dendrimers: pharmacokinetic differences between sizes and cores. *Bioconjugate Chem.* **2003**, *14*, 388−394.
(25) Langereis, S.; de Lussanet, Q. G.; van Genderen, M. H. P.; Backes, W. H.; Meijer, E. W. Multivalent contrast agents based on gadolinium-diethylenetriaminepentaacetic acid-terminated poly-(propyleneimine) dendrimers for magnetic resonance imaging. *Macromolecules* **2004**, *37*, 3084−3091.
(26) Balogh, L.; Tomalia, D. A. Poly(amidoamine) dendrimer-templated nanocomposites. 1. Synthesis of zero valent copper nanoclusters. *J. Am. Chem. Soc.* **1998**, 120, 7355−7356.
(27) Zhao, M.; Sun, L.; Crooks, R. M., Preparation of Cu nanoclusters within dendrimer templates. *J. Am. Chem. Soc.* 1**998**, *120,* 4877−4878.
(28) Zhao M. Q.; Crooks R. M. Intradendrimer exchange of metal nanoparticles. *Chem. Mater.* **1999**, *11*, 3379−3385.
(29) Esumi, K.; Hosoya, T.; Suzuki, A.; Torigoe, K. Spontaneous formation of gold nanoparticles in aqueous solution of sugar-persubstituted poly(amidoamine) dendrimers. *Langmuir* **2000**, *16*, 2978−2980.
(30) Balogh, L.; Swanson, D. R.; Tomalia, D. A.; Hagnauer, G. L.; McManus, A. T.; Dendrimer−silver complexes and nanocomposites as antimicrobial agents. *Nano Lett.* **2001**, *1,* 18−21.
(31) He J. A.; Valluzzi, R.; Yang, K.; Dolukhanyan, T.; Sung, C. M.; Kumar, J.; Tripathy, S. K.; Samuelson, L.; Balogh, L.; Tomalia, D. A. Electrostatic multilayer deposition of a gold−dendrimer nanocomposite. *Chem. Mater*. **1999**, *11*, 3268−3274.
(32) Crooks R M.; Zhao, M. Q.; Sun, L.; Chechik, V. and Yeung, L. K. Dendrimer-encapsulated metal nanoparticles: synthesis, characterization, and application to catalysis. *Acc. Chem. Res.* **2001**, *34*, 181−190.
(33) Wilson, O. M.; Scott, R. W. J.; Garcia-Martinez, J. C.; Crooks, R. M. Separation of dendrimer-encapsulated Au and Ag nanoparticles by selective extraction. *Chem. Mater*. **2004**, *16*, 4202−4204.
(34) Lang, H. G.; Maldonado, S.; Stevenson, K. J.; Chandler, B. D. Synthesis and characterization of dendrimer templated supported bimetallic Pt−Au nanoparticles. *J. Am. Chem. Soc.* **2004**, *126*, 12949−12956.
(35) Sun, X. P.; Dong, S. J.; Wang, E. K. One-step preparation and characterization of poly(propyleneimine) dendrimer-protected silver nanoclusters. *Macromolecules* **2004**, *37*, 7105−7108.
(36) Sun, L.; Crooks, R. M. Interactions between dendrimers and charged probe molecules. 1. Theoretical methods for simulating proton and metal ion binding to symmetric polydentate ligands. *J. Phys. Chem. B* **2002**, *106*, 5864−5872.
(37) Tanford, C. *Physical Chemistry of Macromolecules*; John Wiley & Sons: New York, 1961.
(38) Martell, A. E.; Hancock, R. D. *Metal Complexes in Aqueous Solutions*; Plenum Press: New York, 1996.
(39) Diallo, M. S. Water Treatment by Dendrimer Enhanced Filtration. U.S. Patent Pending.
(40) Harreis, H. M.; Likos, C. N. Can dendrimers be viewed as compact colloids? A simulation study of the fluctuations in a dendrimer of fourth generation. *J. Chem. Phys.* **2003**, *118*, 1979−1988.
(41) Rathgeber, S.; Monkenbusch, M.; Kreitschmann, M.; Urban, V.; Brulet, A. Dynamics of star-burst dendrimers in solution in relation to their structural properties. *J. Chem. Phys.* **2002**, 117, 4047−4062.
(42) Richards, E. G. *An Introduction to Physical Properties of Large Molecules in Solution*; IUPAB Biophysics Series: New York, 1980.
(43) Maiti, P. K, Cagin, T., Wang, G. F., Goddard, W. A. Structure of PAMAM dendrimers: generations 1 through 11. *Macromolecules* **2004**, *32*, 6236−6254.
(44) Armstrong, J. K.; Wenby, R. B.; Meiselman, H. J.; Fisher, T. C. The hydrodynamic radii of macromolecules and their effect on red blood cell aggregation. *Biophys. J.* **2004**, *87*, 4259−4270.
(45) Dvornic, P. R.; Uppuluri, S. Rheology and solution properties of dendrimers. In *Dendrimers and Other Dendritic Polymers*; Fréchet, J. M. J., Tomalia, D. A., Eds.; Wiley and Sons: New York, 2001.
(46) Bowen, R. W.; Doneva, T. A. Atomic force microscopy characterization of ultrafiltration membranes: correspondence between surface pore dimensions and molecular weight cut-off. *Surf. Interface Anal.* **2000**, *29*, 544−547.
(47) Zeman, L. J.; Zydney, A. L. *Microfiltration and Ultrafiltration. Principles and Applications*; Marcel Dekker: New York, 1996.
(48) Kilduff, J. E.; Mattaraj, S.; Sensibaugh, J.; Pieracci, J. P.; Yuan, Y.; Belfort, G. Modeling flux decline during nanofiltration of

NOM with poly(arylsulfone) membranes modified using UV-assisted graft polymerization. *Environ. Eng. Sci.* **2002**, *19*, 477−495.
(49) IGOR Pro Version 4.0. WaveMetrics. http://www.wavemetrics.com/.
(50) Khulbe, K. C.; Matsuura, T. Characterization of synthetic membranes by raman spectroscopy, electron spin resonance and atomic force microscopy; a review. *Polymer* **2000**, *41*, 1917−1935.
(51) Fritzsche, A. K.; Arevalo, A. R.; Connolly, A. F.; Moore, M. D.; Elings, V.; Wu, C. M. The structure and morphology of the skin of polyethersulfone ultrafiltration membranes: a comparative atomic force microscope and scanning electron microscope study. *J. Appl. Polym. Sci.* **1992**, *45*, 1945−1956.
(52) Zeng, Y.; Wang, Z.; Wan, L.; Shi, Y.; Chen, G.; Bai, C. Surface morphology and nodule formation mechanism of cellulose acetate membranes by atomic force microscopy. *J. Appl. Polym. Sci.* **2003**, *88*, 1328−1335.
(53) Madaeni, S. S. Effect of surface roughness on retention of reverse osmosis membranes. *J. Porous Mater.* **2004**, *11*, 255−263.
(54) Bowen, R. W.; Stoton, J. A. G.; Doneva, T. A. Atomic force microscopy study of ulttrafiltration membranes: solute interactions and fouling in pulp and paper processing. *Surf. Interface Anal.* **2002**, *33*, 7−13.
(55) Li, J.; Piehler, T.; Quin, D.; Baker, J. R. Jr.; Tomalia, D. A. Visualization and characterization of poly(amidoamine) dendrimers by atomic force microscopy. *Langmuir* **2000**, *16*, 5613−5616.
(56) Muller, T. M.; Yablon, D. G.; Karchner, R.; Knapp, D.; Kleinman, M. H.; Fang, H.; Durning, C. J.; Tomalia, D. A.; Turro, N. J.; Flynn, G. W. AFM studies of high-generation PAMAM dendrimers at the liquid/solid interface. *Langmuir* **2002**, *18*, 7452−7455.
(57) Pericet-Camara, R.; Papastavrou, G.; Borkovec, M. Atomic force microscopy study of the adsorption and electrostatic self-organization of poly(amidoamine) dendrimers on mica. *Langmuir* **2004**, *20*, 3264.
(58) Nanoscope Command Reference Manual; Software version 5.12, Revision B; Digital Intruments/Veeco Metrology, 2001.
(59) Roberts, J. C.; Bhalgat, M. K.; Zera, R. T. Preliminary biological evaluation of polyamidoamine (PAMAM) starburst demdrimers. *J. Biomed. Mater. Res.* **1996**, *30*, 53−65.

Received for review July 7, 2004. Revised manuscript received December 9, 2004. Accepted December 17, 2004.

ES048961R